Exploration of Quenching Pathways of Multiluminescent Acenes Using the GRRM Method with the SF-TDDFT Method.

AUTHOR(S):

Suzuki, Satoshi; Maeda, Satoshi; Morokuma, Keiji

CITATION:

Suzuki, Satoshi ...[et al]. Exploration of Quenching Pathways of Multiluminescent Acenes Using the GRRM Method with the SF-TDDFT Method.. The journal of physical chemistry. A 2015, 119(47): 11479-11487

ISSUE DATE:

2015-11-25

URL:

http://hdl.handle.net/2433/207517

THE JOURNAL OF PHYSICAL CHEMISTRY A
Article
pubs.acs.org/JPCA

Exploration of Quenching Pathways of Multiluminescent Acenes Using the GRRM Method with the SF-TDDFT Method

Satoshi Suzuki,[‡] Satoshi Maeda,[§] and Keiji Morokuma*[,‡]

[‡]Fukui Institute for Fundamental Chemistry, Kyoto University, Kyoto 606-8103, Japan
[§]Department of Chemistry, Faculty of Science, Hokkaido University, Sapporo 060-0810, Japan

Supporting Information

ABSTRACT: The quenching pathways were investigated for three types of multiluminescent acene derivatives, which show environment-dependent fluorescence. Spin−flip time dependent density functional theory (SF-TDDFT) combined with the Global Reaction Route mapping (GRRM) strategy is employed to locate minimum-energy conical intersections (MECIs). The energies and geometries of the MECIs relative to the Franck−Condon (FC) state control the difference in fluorescence behavior among the three derivatives. For the molecule with a phenyamide moiety, a MECI with energy lower than the FC state with large geometrical change from V-type to flat structure provides an efficient internal conversion (quenching) pathway in solution. For the same molecule, in a solid, this large geometrical change is inhibited, and the second MECI, with an energy lower than FC but higher than the first MECI requiring only a small geometry change of CH out-of-plane bending, contributes to the quenching. The molecule with the napthaleneimide moiety has only one low-energy MECI that requires large geometrical change from the V-type to flat structure. Although this MECI provides the quenching pathway in solution, in the solid, this large motion is inhibited, and the molecule will stay in the excited state and emit. The molecule with an anthraceneimide moiety has no conical intersection lower than the FC state, and no quenching pathway is available in solution or solid. In addition, in this molecule, at the local minimum of the excited state, the dipole transition to the ground state is allowed, and this molecule prefers emission rather than internal conversion.

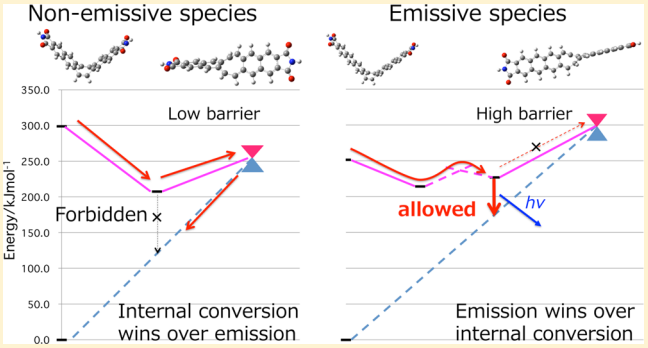

1. INTRODUCTION

Owing to their optical and electronic properties, π-conjugated systems have attracted much attention as a functional material. Recently, a series of π systems that consists of a flexible cyclooctatetraene (COT) core and aceneimide wings with different conjugation lengths has been synthesized.[1,2] This system exhibits bent-to-planar conformal change in the excited state. A significant feature of this system is to show environment-dependent fluorescence from a single-component fluorophore. The system gives a blue emission from the V-shaped structure in a polymer matrix or in a frozen solution, a green emission from the planar geometry in solution, and a red emission in the crystalline state.[1,2] The molecule with anthraceneimide wings is emissive both in solution and in the solid state, while the molecule with phenyleneimide has no emission either in solution or in the solid state. For the molecule with a naphthaleneimide moiety, although no fluorescence is observed in the various common organic solvents at room temperature, the compound shows fluorescence in the solid state. The different emission behavior for different acenes has been explained by the difference in the transition dipole moment (TDM). The TDM of phenyleneimide and naphthaleneimide at the S_1 minimum is zero due to symmetry, while that of anthraceneimide at the S_1 minimum has a finite value. TDM explains why the molecule with an anthraceneimide wing is emissive. However, the difference between phenyleneimide and naphthaleneimide cannot be explained by TDM.

In many photochemical processes such as photochemcial reactions and fluorescence quenching, the conical intersections (CIs) play an important role because nonadiabatic transitions from excited states to the ground state take place very efficiently in the vicinity of the CI.[3−8] The CI between two electronic states forms an $(f - 2)$-dimensional hypersurface, while individual potential energy surfaces (PESs) form f-dimensional hypersurfaces, where f is the internal degree of freedom of a system. Although nonadiabatic transition can take place anywhere near the CI surface, the energy local minimum on the CI hypersurface, the minimum-energy CI (MECI), is a critical point below which CI does not exist and nonadiabatic transition cannot easily take place. In fluorescence, there will be competition between the emission from the local minimum of the excited state controlled by the TDM and quenching through CIs that depends on their geometry, energy, and

Received: August 7, 2015
Revised: October 28, 2015
Published: October 30, 2015

DOI: 10.1021/acs.jpca.5b07682
J. Phys. Chem. A 2015, 119, 11479−11487

nonadiabatic coupling element. If the path from the Franck−Condon (FC) region to reach a CI is downhill or has a low enough barrier, quenching can compete efficiently with fluorescence.

In order to explain the difference in emission behavior of the present molecules, we explored and located MECIs between S_1 and S_0 for the three aceneimides **1**−**3** in Figure 1 and

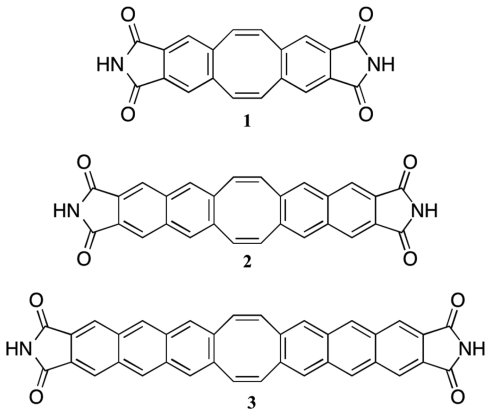

Figure 1. Chemical structure of aceneimide compounds **1**−**3**.

determined possible quenching pathways, starting from the FC region, with the GRRM (Global Reaction Route Mapping) strategy,[9−15] which consists of two independent automatic global search methods, ADDF and AFIR (see ref 12 in detail). The difference in quenching pathway among the three systems would lead to the difference of emission behavior.

Time-dependent density functional theory (TDDFT) is a powerful tool for describing excited states. Among the wave function theories, the multiconfigurational space self-consistent field (MCSCF) method, such as the complete active space self-consistent field (CASSCF), and the multireference perturbation theory, such as the second-order complete active space perturbation theory (CASPT2)[16] and multiconfigurational quasidegenerate perturbation theory (MCQDPT),[17] have been widely used to calculate excited states. CASSCF lacks dynamic correlation and sometimes fails to describe electronic structure properly. The multireference perturbation theory includes dynamic electronic correlation and is usually reliable, but its computational cost is sometimes too large to apply to large molecular systems.

On the other hand, TDDFT is very useful for many cases owing to its "acceptable" accuracy and low computational cost. In the linear response (LR)-TDDFT, excitation energies are determined as poles of the response function. Because the ground state and excited states are treated in a different way, the CI between them cannot be determined in the TDDFT method.

Recently, it has been shown that spin−flip (SF)-TDDFT has a potential ability to obtain the correct CI.[18−21] In SF-TDDFT, S_0 and S_1 states are expressed as excited states from the reference lowest triplet T_1 state that is obtained in the unrestricted Kohn−Sham (UKS) or restricted open-shell Kohn−Sham (ROKS) equation. In the present calculation, ROKS is employed. A significant fault of the SF-TDDFT method is that it often gives spin-contaminated states. To deal with this problem, we checked $\langle \mathbf{S}^2 \rangle$ and the CI coefficients during the optimization. Details are described in a later section.

Section 2 describes the theoretical background and computational methods. In section 3, quenching pathways of each molecule are determined and discussed. The conclusion is given in section 4.

2. METHODS AND COMPUTATIONAL DETAILS

In the experiment, *n*-butylimides are used. In the present study, *n*-butyl groups are replaced by hydrogens. Preliminary calculations suggested that the effect of *n*-butyl on the structure and excitation energies is not very significant. For instance, the lowest excitation energy is 2.73 eV with *n*-butyl, while it is 2.72 eV with H. Therefore, this replacement can be justified for qualitative discussion. The equilibrium geometry of each molecule in the S_0 state was optimized at the B3LYP/6-31+G(d) level. Starting from the S_0 equilibrium geometry, the local or global minimum (MIN) for the S_1 state is optimized with TD-B3LYP/6-31+G(d). Throughout the paper, energies and gradients were computed by the GAMESS program.[22]

It turns out that starting the MECI search from the FC geometry by using SF-TDDFT is not necessarily the most efficient as the geometry of MECI is often substantially different from that of the FC geometry and SF-TDDFT states change their nature during optimization. Instead, we used standard restricted and unrestricted DFT methods to calculate S_0 and T_1 states, respectively, and located the approximate minimum-energy point on the seam of crossing (MESX) between S_0 and T_1. One expects that S_0 and T_1 states have similar shape of potential surfaces if they have the same electron configuration (except for spin). Thus, the S_1/S_0 MECI search from S_0/T_1 MESX is finished with a small number of iterations. This MESX search requires only standard DFT calculations for the lowest singlet and lowest triplet states and avoids SF-TDDFT excited-state calculations. After MESXs were obtained, we searched the S_1/S_0 MECI from each S_0/T_1 MESX.

MESXs are located by adopting the ADDF (anharmonic downward distortion following) search method for the seam model function (SMF) method implemented in the GRRM program.[23] It is worth noting that ADDF search is a method to obtain all possible local minima on a PES. Thus, when we apply the ADDF method to SMF, we can locate many lowest local minima on SMF.

SMF is a function

$$F^{\mathrm{SMF}}(\mathbf{Q}) = \frac{1}{2}[E^{\mathrm{State\text{-}1}}(\mathbf{Q}) + E^{\mathrm{State\text{-}2}}(\mathbf{Q})] + \frac{[E^{\mathrm{State\text{-}1}}(\mathbf{Q}) - E^{\mathrm{State\text{-}2}}(\mathbf{Q})]^2}{\alpha} \quad (1)$$

consisting of a mean energy term for the two target PESs, $E^{\mathrm{State\text{-}1}}(\mathbf{Q})$ and $E^{\mathrm{State\text{-}2}}(\mathbf{Q})$, and a penalty function for their energy difference. $\mathbf{Q}$ represents the atomic coordinates $\{Q_i\}$, and α is a constant parameter. Minima of SMF correspond to approximate MESX geometries. For each molecule independently, we obtained all important MESXs without guess using a combination of the SMF and ADDF approach. From all of these MESXs (excluding ones with energy higher than S_1 FC), we optimized MECIs. Thus, it is very unlikely that any important MECI is missed. SF-TDB3LYP/3-21G was used for the initial MESXs search, and S_1/S_0 MECIs were reoptimized using the branching plane updating method[11] at the SF-TDB3LYP/6-31+G(d) level, all using the GRRM program.[22] Energies and gradients of the S_0 and S_1 states were calculated

DOI: 10.1021/acs.jpca.5b07682
J. Phys. Chem. A 2015, 119, 11479−11487

using the SF-TDDFT method with the Tamm−Dancoff approximation implemented in the GAMESS program package. In the SF-TDDFT calculation, the reference triplet state was obtained by the ROKS equation.

One significant fault of SF-TDDFT is that it gives spin-contaminated states. Although expectation values of the total spin-squared operator, namely, $\langle \mathbf{S}^2 \rangle$, sometimes fluctuate between 0.0 and 2.0, which correspond to pure singlet or triplet states, they often become around 1.0, which indicates strongly mixed states. To determine the nature of SF-TDDT states, we checked $\langle \mathbf{S}^2 \rangle$ and the CI coefficients during the optimization. With ROKS, there are two open-shell electrons. These two singly occupied orbitals in the reference triplet state should be HOMO and LUMO in the S_0 state. Let us denote the electron configuration using H and L, which correspond to the HOMO and LUMO, and a and b, which mean α and β spin, respectively. For instance, the reference triplet state becomes HaLa in this notation. The S_0 state should satisfy following two conditions: $\langle \mathbf{S}^2 \rangle \approx 0.0$ and $C^2(\mathrm{HaHb}) \approx 1.0$, where C is a CI coefficient. S_1 consists mainly of the $(\mathrm{HOMO})^1(\mathrm{LUMO})^1$ configurations. Thus, $C^2(\mathrm{HaLb}) + C^2(\mathrm{HbLa})$ is usually around 1.0 for this state. We employed the following scheme for the S_1/S_0 MECI search using the SMF ADDF approach:

(1) Starting from ROKS triplet state, obtain the three lowest states by SF-TDDFT. These three states usually are S_0, S_1, and T_1.

(2) Calculate the following T index value for each state[13]

$$T = \langle \mathbf{S}^2 \rangle + C^2(\mathrm{HaHb}) + C^2(\mathrm{HaLb}) + C^2(\mathrm{HbLa}) + C^2(\mathrm{LaLb}) \quad (2)$$

The T index should be 3 and 1 for pure $(\mathrm{HOMO})^1(\mathrm{LUMO})^1$ triplet and singlet states, respectively, and 1 for pure $(\mathrm{HOMO})^2$ and $(\mathrm{LUMO})^2$ closed-shell singlet states. This would be 1 for states originating from excitations outside of the 2 × 2 (HOMO) (LUMO) configuration space; such states are mixtures of singlet and triplet states by the nature of the SF-TDDFT method.

(3) Compare three T values of the lowest three SF-TDDFT states; states with two smaller T values are judged to correspond to singlet-like states.

(4) Calculate the energy gradients for singlet-like states and generate the next geometry for the S_1/S_0 MECI search.

This state selection scheme based on the T value does not change the wave function and thus does not avoid spin contamination during geometry optimization. However, near the FC geometry and S_1/S_0 CI, the pure triplet state within the 2 × 2 active space is automatically excluded.

After an S_1/S_0 MECI is obtained, meta-IRC[24] (mass-weighted steepest descent path) calculation on the S_0 state from this MECI was performed to check the direct (without barrier) connectivity of MECI to the S_0 minimum. Geometry optimization on S_1 from the FC geometry as well as that from each MECI was also performed to check whether the FC and the MECI geometries are connected directly (without barrier) to the S_1 minimum. The results will be discussed for each system in the Results and Discussion section.

3. RESULTS AND DISCUSSION

3.1. Determination of Critical Points for Molecules 1−3.

Molecule 1. Figure 2 shows the structure of important critical points and their energies for molecule **1**. Table 1 shows essential geometrical parameters, CC bond distances, and CCCX (X = C, H) dihedral angles of these critical points, and Table 2 gives electronic structure characteristics for these critical points, such as the $\langle \mathbf{S}^2 \rangle$ value, CI coefficients, and T index.

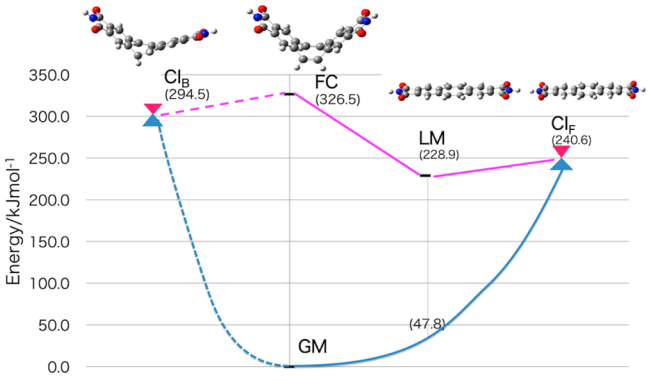

Figure 2. Potential energy profile of molecule **1**. Solid lines mean that connections between points are confirmed by meta-IRC or geometry optimization. Connections with dotted lines are not confirmed.

A local minimum **LM** on the S_1 surface is found near the C_{2v} **FC** point (the ground-state minimum **GM**) with a planar symmetric D_{2h} structure, in which the C2═C3 and weaker C4═C5 double bond characters of the S_0 state **GM** are qualitatively retained, as seen in Table 1. The gradient at **FC** on S_1 is sloped to the direction of **LM**, and the meta-IRC from **FC** confirms that **LM** is reached without barrier. **LM** is 97.6 kJ mol^{-1} lower than **FC**. The electronic structure characteristics of S_1 at **LM** in Table 2 indicate that this state is somewhat spin-contaminated, but it can still be assigned to a singlet state. Actually, a triplet T_1 state is relatively close to the S_1 state at this geometry, which causes spin contamination. However, the shape of the S_1 and T_1 PESs would not be much affected by spin mixing.

The optimized MECI $\mathbf{CI_F}$ also has a planar symmetric D_{2h} geometry. Comparing with the geometries of **GM** and **LM**, $\mathbf{CI_F}$ shows a profound bond alternation; C1−C2 and the other corresponding bonds became short, and C2−C3 and C4−C5 and the other corresponding bonds became long, totally opposite to the bond character of **GM** and **LM**. Thus, one can say that this MECI created is due to the bond alternation of the COT ring. The bond alternation lowers the energy of S_1 and at the same time raises the energy of S_0, resulting in CIs. $\mathbf{CI_F}$ is lower in energy than **FC** by 85.9 kJ mol^{-1} and is higher than **LM** only by 11.7 kJ mol^{-1}. The meta-IRC calculations from **FC** and $\mathbf{CI_F}$ on the S_1 surface confirm that both **FC** and $\mathbf{CI_F}$ are connected to **LM** downhill on S_1 without a barrier. The meta-IRC calculation from $\mathbf{CI_F}$ on the S_0 surface also confirms that $\mathbf{CI_F}$ is connected to **GM** downhill on S_0 without a barrier.

We also found a different type of MECI, $\mathbf{CI_B}$, which is 32.0 kJ mol^{-1} lower than **FC**. We did not explore the lowest-energy path from **FC** to $\mathbf{CI_B}$. However, TDDFT calculations along optimization steps between $\mathbf{CI_B}$ and **GM** on the S_0 surface suggest that the barrier between them would not exceed 20.0 kJ mol^{-1} relative to FC. Therefore, $\mathbf{CI_B}$ is less favored than $\mathbf{CI_F}$, but it is still reachable on the S_1 surface starting from the **FC** energy and geometry. An optimization from $\mathbf{CI_B}$ on S_0 suggests that $\mathbf{CI_B}$ is connected to **GM** on S_0 without a high barrier.

This $\mathbf{CI_B}$ with C_1 symmetry shows large out-of-plane bending of two neighboring CH bonds in COT. The dihedral angle C5−C6−C7−Hd is 81.9°, with Hd almost perpendicular to the COT C5−C6−C7 plane, and the C8−C7−C6−Hc and C4−

DOI: 10.1021/acs.jpca.5b07682
J. Phys. Chem. A 2015, 119, 11479−11487

Table 1. Important CC Bond Distances and CCCX (X = C, H) Dihedral Angles at the S_0 Global Minimum (FC), S_1 Local Minima (LMs), and S_1/S_0 MECIs (CIs) of Molecules 1−3

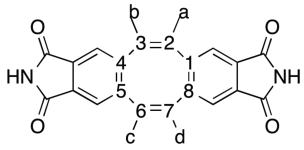

molecule				1				2			3			
structure				FC	LM	CI_F	CI_B	FC	LM	CI	FC	LM_V	LM_F	CI
Dihedral Angle (deg)														
1	2	3	4	0.0	0.0	0.0	−1.0	0.0	0.0	60.6	0.0	0.0	0.0	69.9
2	3	4	5	−58.5	0.0	0.0	−14.1	−57.1	0.0	1.4	−56.4	−38.9	0.0	−0.2
3	4	5	6	0.0	0.0	0.0	−29.7	0.0	0.0	−41.3	0.0	0.0	0.0	−42.1
4	5	6	7	58.5	0.0	0.0	115.1	57.1	0.0	−15.8	56.4	38.9	0.0	−20.7
5	6	7	8	0.0	0.0	0.0	−96.4	0.0	0.0	60.6	0.0	0.0	0.0	70.0
6	7	8	1	−58.5	0.0	0.0	6.1	−57.1	0.0	1.4	−56.4	−38.9	0.0	−0.2
7	8	1	2	0.0	0.0	0.0	18.7	0.0	0.0	−41.3	0.0	0.0	0.0	−42.1
8	1	2	3	58.5	0.0	0.0	6.7	57.1	0.0	−15.8	56.4	38.9	0.0	−20.7
8	1	2	a	−127.6	180.0	180.0	179.5	−129.2	180.0	−177.6	−130.2	−150.5	180.0	178.9
5	4	3	b	127.6	180.0	180.0	174.0	129.2	180.0	−170.5	130.2	150.5	180.0	−172.7
4	5	6	c	−127.6	180.0	180.0	−19.2	−129.2	180.0	−177.5	−130.2	−150.5	180.0	−178.9
1	8	7	d	127.6	180.0	180.0	−172.3	129.2	180.0	−170.6	130.2	150.5	180.0	−172.7
4	3	2	a	−173.7	180.0	180.0	−173.8	−173.6	180.0	−137.3	−173.3	−170.6	180.0	−129.2
1	2	3	b	173.7	180.0	180.0	171.0	173.6	180.0	−127.3	173.3	170.6	180.0	−117.5
8	7	6	c	−173.7	180.0	180.0	37.9	−173.6	180.0	−137.3	−173.3	−170.6	180.0	−129.2
5	6	7	d	173.7	180.0	180.0	81.9	173.6	180.0	−127.3	173.3	170.6	180.0	−117.4
Bond Distance (Å)														
1	2			1.422	1.473	1.359	1.422	1.481	1.415	1.374	1.480	1.455	1.424	1.366
2	3			1.428	1.353	1.468	1.428	1.344	1.403	1.452	1.344	1.364	1.400	1.465
3	4			1.410	1.473	1.362	1.410	1.481	1.415	1.372	1.480	1.455	1.424	1.369
4	5			1.462	1.430	1.521	1.462	1.432	1.478	1.488	1.444	1.437	1.474	1.489
5	6			1.406	1.472	1.359	1.406	1.481	1.415	1.374	1.480	1.455	1.419	1.366
6	7			1.437	1.353	1.468	1.437	1.344	1.403	1.452	1.344	1.364	1.397	1.465
7	8			1.389	1.472	1.362	1.389	1.481	1.415	1.372	1.480	1.455	1.419	1.369
8	1			1.497	1.430	1.521	1.497	1.432	1.478	1.488	1.444	1.437	1.474	1.489
symmetry				C_{2v}	D_{2h}	D_{2h}	C_1	C_{2v}	D_{2h}	C_2	C_{2v}	C_{2v}	C_{2v}	C_2

Table 2. $\langle S^2 \rangle$ Value, CI Coefficients, and *T* Index Values for S_0 and S_1 States at the S_0 Global Minimum (FC), S_1 Local Minima (LMs), and S_1/S_0 MECIs (CIs) of Molecules 1−3

molecule		1				2			3			
structure		FC	LM	CI_F	CI_B	FC	LM	CI	FC	LM_V	LM_F	CI
	$\langle S^2 \rangle$	0.003	0.005	0.410	0.148	0.013	0.009	0.030	0.015	0.005	0.013	0.015
S_0	CI(HaHb)	0.999	−0.998	−0.821	−0.938	−0.994	0.997	−0.459	−0.992	0.998	−0.993	0.836
	CI(HaLb)	0.000	0.000	0.556	−0.137	0.000	0.000	−0.671	0.000	0.000	0.000	0.382
	CI(HbLa)	0.000	0.000	0.079	−0.094	0.000	0.000	0.571	0.000	0.000	0.000	−0.379
	CI(LaLb)	0.000	0.000	−0.080	0.000	0.000	0.000	0.000	0.000	0.000	0.000	0.000
	T index	1.001	1.001	1.405	1.056	1.000	1.001	1.001	1.001	1.001	1.001	1.001
	$\langle S^2 \rangle$	0.062	0.088	0.253	0.930	1.013	0.079	0.015	0.308	1.002	1.061	0.067
S_1	CI(HaHb)	0.000	0.000	−0.188	−0.104	0.000	0.000	0.882	0.000	0.000	0.000	−0.537
	CI(HaLb)	0.578	0.549	0.000	0.980	0.000	0.562	−0.312	−0.597	0.000	−0.189	0.000
	CI(HbLa)	−0.813	−0.833	0.891	0.000	0.000	−0.823	0.338	0.584	0.000	−0.130	−0.498
	CI(LaLb)	0.000	0.000	−0.403	0.065	0.000	0.000	0.000	0.000	0.000	0.000	0.665
	T index	1.057	1.083	1.244	1.906	1.013	1.071	1.005	1.006	1.002	1.114	1.046

C5−C6−Hc are 37.9 and −19.2°, respectively, with the Hc very much twist-bent from the COT C5−C6−C7 plane (Table 1). A CI similar to this has been found for COT[25] and is also similar to the twisted CI of stilbene.[20,26] As seen in Table 2, at this CI, S_1 and T_1 are strongly spin-contaminated; $\langle S^2 \rangle$ for the S_1 and T_1 states is 0.93 and 1.05, respectively (Table 2). The *T* index for the SF-TDDFT state 2 is smaller than that of state 3, and hence, state 2 is assigned to S_1 and state 3 to T_1. Because the energy difference between states 2 and 3 is only 28 kJ mol^{-1}, the crossing between S_0 and the spin-pure S_1 state should have a similar geometry to the crossing structure obtained for the heavily spin-mixed state. To examine these states, single-point (4,4) CASSCF calculation is also performed. HOMO−1, HOMO, LUMO, and LUMO+1 are taken into

DOI: 10.1021/acs.jpca.5b07682
J. Phys. Chem. A 2015, 119, 11479−11487

Table 3. Energy, $\langle S^2 \rangle$ Value, CI Coefficients, and *T* Index Values for T_1, S_0, S_1, and T_2 States of SF-TDDFT at the S_1/S_0 MECI (CI_B) of Molecule 1 along with (4,4)-CASSCF Energy and CI Coefficients for S_0, T_1, and S_1 States at the Same Geometry

	SF-TDDFT				2SA-(4,4)CASSCF		
	T_1 (ROKS state)	S_0	S_1	T_1	S_0	T_1	S_1
ΔE(kJ/mol)	0.0	30.5	30.5	58.4	0.0	26.0	60.1
$\langle S^2 \rangle$	2	0.1482	0.9301	1.0531	0	2	0
CI(HaHb)	0.0000	−0.9380	−0.1043	0.1132	−0.0769	0.0000	0.9046
CI(HaLb)	0.0000	−0.1368	0.9801	0.0000	0.6238	−0.6068	0.0000
CI(HbLa)	0.0000	−0.0944	0.0000	−0.9626	0.6238	0.6068	0.0000
CI(LaLb)	0.0000	0.0000	0.0653	0.0581	0.0000	0.0000	0.1349
T index		1.056	1.906	1.996			

active orbitals, and S_0 and S_1 states are averaged. As shown in Table 3, the S_0 state in SF-TDDFT corresponds to the S_1 state in CASSCF. On the other hand, S_1 and T_1 states in SF-TDDFT correspond to linear combinations of S_0 and T_1 states in CASSCF. This reflects the fault of the SF-TDDFT method; for more quantitative description of these states, a more accurate and contamination-free method such as CASPT2 is needed.

Interestingly, at both $\mathbf{CI_F}$ and $\mathbf{CI_B}$, deformation mainly takes place on the COT ring. In a preliminary calculation with a small basis set, we also found other CIs with out-of-plane CH bending of benzene ring hydrogens. However, these types of CIs have much higher energy and will not contribute to the quenching of luminescence, and therefore, such CIs will not be discussed in the present paper. The reason why the deformation takes place on the COT ring comes from the nature of the excited state. Figure 3 shows two singly occupied

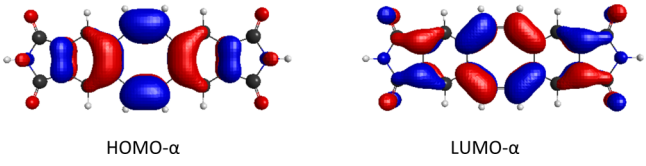

Figure 3. Two singly occupied orbitals (called HOMO-α and LUMO-α) from the ROKS triplet reference calculation at the S_1 **LM** geometry of molecule **1**.

orbitals (called HOMO-α and LUMO-α) from the ROKS triplet reference calculation at the S_1 **LM** geometry of molecule **1**. These MOs are mainly localized in the COT ring and clearly represent bond alternation within the COT ring upon excitation from the HOMO to LUMO in S_1. A small density on the phenyl carbon next to the COT ring suggests that bending of this CH bond may result in a high-energy CI.

Molecule 2. Figure 4 and Table 1 show the structure of important critical points and their energies for molecule **2**. For molecule **2**, a local minimum **LM** with D_{2h} symmetry is found on S_1, which is similar to the S_1 local minimum **LM** of **1**. Comparing these two molecules, we can see some differences in bond distances. In molecule **1**, bond distances of 1−2, 2−3, and 4−5 are 1.473, 1.353, and 1.430 Å, respectively. In molecule **2**, they are 1.415, 1.403, and 1.478 Å, respectively; the bond distance alternation is very much reduced.

On the other hand, the structure of MECI **CI** is quite different from either of the two MECIs, $\mathbf{CI_F}$ and $\mathbf{CI_B}$, of molecule **1**. At this **CI**, the COT has made a major structural change from the S_0 **GM**. The larger V-shaped bend of the COT ring in the S_0 **GM** has disappeared completely and been replaced by a C_2 pseudo-tub-shaped conformation of COT with aryl groups attached on the side of the tub (Figure 5). This

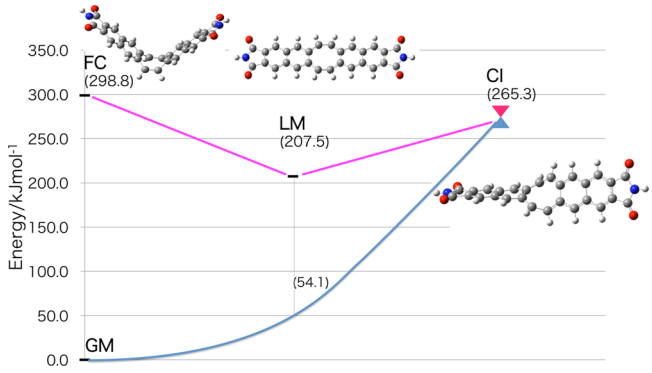

Figure 4. Potential energy profile of molecule **2**. Solid lines mean that connections between points are confirmed by meta-IRC or geometry optimization. Connections with dotted lines are not confirmed.

distortion is quite different from those of **1**, $\mathbf{CI_F}$ promoted by bond alternation, and $\mathbf{CI_B}$ associated with the C−H out-of-plane bending.

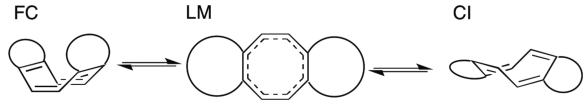

Figure 5. Schematic representation of critical points of molecule **2**.

Another flat CI, similar to $\mathbf{CI_F}$ of **1**, may also exist. We also tried to find such a CI from **LM**, but finally we obtained only this pseudo-tub **CI**. We conclude that such a flat CI in molecule **2** does not exist or is substantially higher in energy. This **CI** for molecule **2** is lower than the S_1 **FC** by 33.5 kJ mol^{-1} but 57.8 kJ mol^{-1} higher than S_1 **LM**. Although the required energy is not so small, this **CI** is still accessible from **FC**. The meta-IRC calculations from **FC** and **CI** on the S_1 surface confirm that both **FC** and **CI** are connected to **LM** downhill on S_1 without a barrier. The meta-IRC calculation from **CI** on the S_0 surface also confirms that **CI** is connected to **GM** downhill on S_0 without a barrier.

Different from **1**, the pseudo-tub-shaped **CI** is the only MECI lower than **FC**. In preliminary calculation with a small basis set, we also found other CIs that have strong CH out-of-plane bending as in $\mathbf{CI_B}$ of **1**. However, this CI is much higher in energy than **FC**. Thus, we will not considered these high-energy CIs in the later discussion.

Table 2 indicates that both **LM** and **CI** are nearly pure singlet states with small $\langle S^2 \rangle$ values and the *T* indices of nearly 1. At **LM**, S_0 is a closed shell, and S_1 is an open-shell singlet, and at **CI**, the two singlets are fully mixed.

DOI: 10.1021/acs.jpca.5b07682
J. Phys. Chem. A 2015, 119, 11479−11487

Molecule **3**. There is a noticeable difference between molecule **3** and molecules **1** and **2**. For molecule **3**, two C_{2v} local minima for S_1 state were found (Figure 6 and Table 2). As

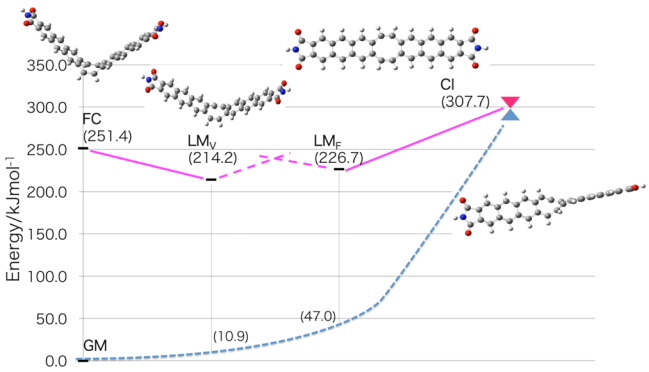

Figure 6. Potential energy profile of molecule **3**. Solid lines mean that connections between points are confirmed by meta-IRC or geometry optimization. Connections with dotted lines are not confirmed.

found previously,[2] there is one local minimum $\mathbf{LM_V}$ that has a shallow V shape and another local minimum $\mathbf{LM_F}$ with flat C_{2v} geometry. $\mathbf{LM_V}$ is lower in energy by 12.5 kJ mol^{-1} than $\mathbf{LM_F}$. This is different from a previous study, in which relaxed scan found $\mathbf{LM_F}$ slightly lower than $\mathbf{LM_V}$.[2] Because the differences between two geometries are as small as the typical error of TDDFT (around 0.1 eV, namely, 10 kJ mol^{-1}),[27] we will not discuss this difference further.

At the **FC** C_{2v} V-shaped structure, the lowest singlet excited state S_1 is $^1A_2$. Following the meta-IRC from **FC**, $\mathbf{LM_V}$, still with a V-shaped structure with a smaller bending angle, is reached with $^1A_2$ as S_1. As the molecule become even more planar, $^1B_2$ becomes lower than $^1A_2$. At the second S_1 minimum $\mathbf{LM_F}$, the molecule is coplanar, and the first excited state is $^1B_2$. The electronic transition (emission) from $^1B_2$ to S_0 ($^1A_1$) is allowed, while that from $^1A_2$ to S_0 is forbidden. Thus, molecule **3** can give emission from the second S_1 minimum $\mathbf{LM_F}$ but not from the first minimum $\mathbf{LM_V}$. The calculated vertical emission energy (without zero-point energy correction) from $\mathbf{LM_F}$ is 179 kJ mol^{-1}, while that of experiment in solution is 230 kJ mol^{-1} (520 nm).

Between the two minima $\mathbf{LM_V}$ and $\mathbf{LM_F}$, there should be a transition state due to avoided crossing of the two electronic states. It is not easy to describe this avoided crossing with the SF-TDDFT method, and a search based on SF-TDDFT did not give a reliable TS structure. However, from an approximate scan of the two states, one can say that the barrier between $\mathbf{LM_V}$ and $\mathbf{LM_F}$ would be less than 20 kJ mol^{-1}. The process going from **FC** though $\mathbf{LM_V}$ to $\mathbf{LM_F}$ would be a viable step.

In molecule **3**, the COT moiety is antiaromatic in the ground state. Thus, conjugation is divided into two parts. On the other hand, at the $\mathbf{LM_F}$, the COT moiety becomes planar, and conjugation becomes enlarged to the whole system. This delocalization stabilizes the $^1B_2$ state, and the order of excited states is switched.

One MECI, labeled **CI**, has been found for molecule **3**. **CI** is higher in energy than the FC structure **FC** by 56.3 kJ mol^{-1}. This structure **CI** consists of two nearly planar acene structures that are connected by a nearly perpendicularly twisted COT structure, similar to the **CI** structure of **2**. A flat CI like **1** could not be found, which is the same result as **2**. It is interesting to follow the structure change of molecule **3** on S_1: deeply V-shaped **FC**, followed by shallowly V-shaped $\mathbf{LM_V}$, coplanar $\mathbf{LM_F}$, and twisted **CI**.

One notices that **CI** of molecule **2** is *lower* than **FC** by 33.5 kJ mol^{-1}, while **CI** of molecule **3** is *higher* than **FC** by 56.3 kJ mol^{-1}. As shown in Table 1, structures of **CI** for **2** and **3** are similar. Thus, it is difficult to explain this energy difference from a structural point of view. To verify electronic structure at CIs, we performed S_0/S_1 state-average (4,4) CASSCF/6-31+(d) single-point calculation at the MECI **CI** for both molecule **2** and **3**. In Figure 7, four natural orbitals (NOs) of **2** and **3** are

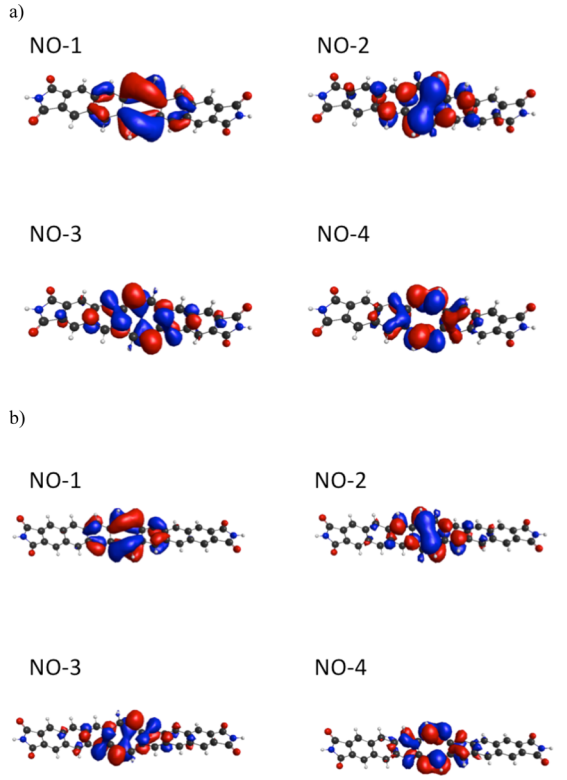

Figure 7. (a) Two-state SA (4,4) CASSCF NOs at **CI** for molecule **2**. The occupation number for each NO for state 1 is 1.882, 1.405, 0.612, and 0.100, respectively. (b) Two-state SA (4,4) CASSCF NOs at **CI** for molecule **3**. The occupation number for each NO is 1.799, 1.329, 0.705, and 0.167, respectively.

shown (isovalues = 0.025). Apparently, their orbitals are very similar, and the natural orbital occupation numbers (NOONs) are also similar. For molecule **2**, the NOON for each NO is 1.882, 1.405, 0.612, and 0.100, respectively; for molecule **3**, the NOON for each NO is 1.799, 1.329, 0.705, and 0.167, respectively. We can conclude that the difference between electronic structures on **CI** for **2** and **3** is not large enough to explain energetics on CI.

One significant difference, as shown in Figure 8, between **2** and **3** is the symmetry of LMs. As shown in Table 1, **LM** for **2** is a rectangle belonging to D_{2h}, while $\mathbf{LM_F}$ for **3** loses C_2 symmetry around the *z*-axis and is a trapezoid belonging to C_{2v}. On the other hand, the CIs for both **2** and **3** are a twisted rectangle, possessing C_2 rotational symmetry around the *z*-axis. Now, we introduce for **3** a hypothetical D_{2h} structure $\mathbf{H_{D2h}}$, by symmetrizing the $\mathbf{LM_F}$ C_{2v} structure. The energy difference between **CI** and $\mathbf{LM_F}$ can now be rewritten as

DOI: 10.1021/acs.jpca.5b07682
J. Phys. Chem. A 2015, 119, 11479−11487

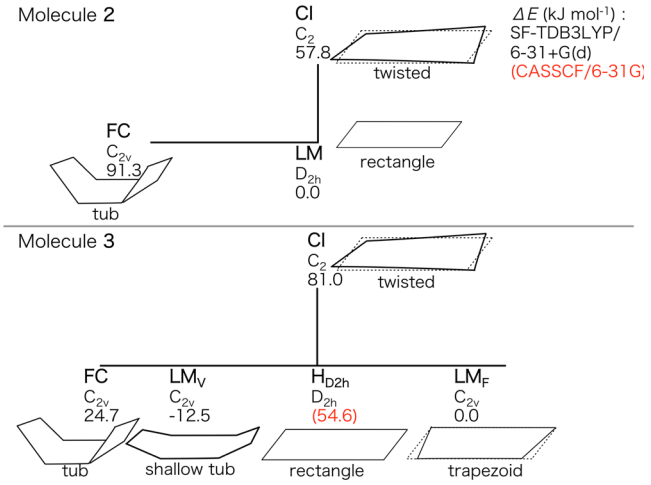

Figure 8. Schematic illustration of geometries (symmetries) and energies of critical points of molecules **2** and **3**, at the SF-TDB3LYP/6-31+G(d) level, except for the red number in CASSCF/6-31G. See the text for details.

$$E(\mathbf{CI}) - E(\mathbf{LM_F}) = [E(\mathbf{CI}) - E(\mathbf{H_{D2h}})] + [E(\mathbf{H_{D2h}}) - E(\mathbf{LM_F})] \quad (3)$$

This divides the $\mathbf{LM_F}$ to **CI** geometry change into the trapezoid-to-rectangle deformation ($\mathbf{LM_F}$ to $\mathbf{H_{D2h}}$) and the twisting of the rectangle ($\mathbf{H_{D2h}}$ to **CI**). Unfortunately, the SF-TDDFT calculation at $\mathbf{H_{D2h}}$ did not converge. Therefore, instead, we estimated the energy of the hypothetical D_{2h} structure $\mathbf{H_{D2h}}$ as follows. $\mathbf{LM_F}$ was optimized with state-specific (4,4)-CASSCF/6-31G for the S_1 state ($^1B_2$ in C_{2v} symmetry), and then the D_{2h} structure $\mathbf{H_{D2h}}$ was obtained by symmetry-constrained optimization with the same method as that for the S_1 state (^1Ag). The energy difference between $\mathbf{H_{D2h}}$ and $\mathbf{LM_F}$, the stabilization energy due to rectangle-to-trapezoid distortion, is calculated to be 54.6 kJ mol^{-1} at this level. Therefore, one can conclude that the **CI**−**LM** energy difference in molecule **3** is much larger than that in molecule **2** because $\mathbf{LM_F}$ of **3** is stabilized by 54.6 kJ mol^{-1} from the hypothetical rectangular structure and corresponding electronic structure, while **LM** of **2** already has a rectangular structure. Molecule **2** in the **LM** structure in the S_1 excited state prefers to keep each of the smaller naphthalene groups symmetric around the COT core, while molecule **3** in the $\mathbf{LM_F}$ structure in the S_1 excited state prefers to distort each of the larger anthracene groups into a trapezoid.

3.2. Quenching Pathway for Three Types of Molecule.

In molecule **1**, as seen in Figure 2, after vertical excitation, the minim-energy path takes the system preferentially to the S_1 **LM**. The electronic transition (emission) from S_1 to S_0 is forbidden by symmetry, and the molecule cannot emit from S_1 **LM**. From **LM**, the molecule moves easily to the MECI $\mathbf{CI_F}$, through which it moves on to the S_0 ground state to reach the S_0 global minimum. This quenching pathway is driven by the large geometry from the V shape in **FC** to the coplanar shape in **LM** and $\mathbf{CI_F}$. This geometry change is accompanied by the COT bond alternation caused by electronic excitation. This quenching pathway should be the most preferable in solution and is likely to occur in high probability as the meta-IRC on S_1 from **FC** leads to **LM** and to $\mathbf{CI_F}$ without any barrier. In addition, there is another MECI $\mathbf{CI_B}$ in the different direction of geometry distortion. Although $\mathbf{CI_B}$ is also lower in energy than **FC**, the pathway toward $\mathbf{CI_B}$ from **FC** is not on the steepest decent path and should be accessible from **FC** with some activation energy. This path not on the minimum-energy pathway may contribute but is not likely to compete against the steepest descent quenching path via MECI $\mathbf{CI_F}$ in the gas phase or in solution.

In solid, however, large structural changes should be inhibited by the surroundings. Thus, $\mathbf{CI_F}$ that requires a large geometry change from the **FC** V structure to a planar structure may not be reachable. However, $\mathbf{CI_B}$ is lower in energy than **FC** and requires relatively small structural change (a CH out-of-plane bending retaining the V-shape structure). Thus, $\mathbf{CI_B}$ is expected to be reachable even in the solid state. Therefore, we propose that the quenching of molecule **1** via $\mathbf{CI_B}$ is still possible in solid, explaining qualitatively the experimental finding of no emission either in solution or in solid for molecule **1**.

On the other hand, in molecule **2**, there is only one type of MECI, **CI**, with lower energy in the vicinity of **FC**. No CI for **2**, similar to $\mathbf{CI_B}$ in molecule **1**, could not be located in the GRRM SMF search, suggesting that this, if it exists, is substantially higher in energy than **FC**. The electronic transition (emission) from S_1 to S_0 is forbidden by symmetry and should be weak. The molecule **2** moves easily to the MECI **CI**, through which the molecule moves on to the S_0 ground state to reach the S_0 ground minimum, as in molecule **1**. This should be the favorable quenching pathway in the gas phase and in solution. As discussed for molecule **1**, this pathway of quenching would be prohibitive in solid also for molecule **2.** This pathway from the V-shape **FC** through coplanar **LM** to twisted **CI** requires a large geometrical change and will be inhibited by surroundings. The above argument qualitatively explains why molecule **2** is nonemissive in solution and is only weakly emissive in solid.

In molecule **3**, the situation is totally different from **1** and **2**. At $\mathbf{LM_F}$, the transition between S_1 and S_0 is allowed by symmetry. In addition, the barrier toward **CI** is high enough. Thus, in this molecule, fluorescence is more likely to take place than internal conversion in either the solution or solid, consistent with experimental observations.

4. CONCLUSION

We have explored quenching pathways of three multi-luminescent molecules using SF-TDDFT in conjunction with the GRRM ADDF automatic search method for MECI and proposed different quenching mechanisms for three different molecules **1**, **2**, and **3**. As a referee suggested, it may be hard to believe that the photochemistry of these structurally similar molecules is qualitatively as different as reported. A standard search from a guess would have missed this difference. The unbiased and global search of MECIs by the GRRM ADDF method demonstrated that dramatic change in MECI characteristics and emission behavior is exactly what is taking place going from molecule **1** to **2** to **3**.

Molecule **1** with phenyleneimide has two low-energy MECIs, $\mathbf{CI_F}$ and $\mathbf{CI_B}$. In contrast to the strongly V-shaped FC structure **FC**, $\mathbf{CI_F}$ has a flat structure and is lower than **FC** by 86 kJ mol^{-1} and is connected via the local minimum **LM** (12 kJ mol^{-1} lower than $\mathbf{CI_F}$) to **FC** directly without barrier. Thus, the excited molecule should be quenched very easily in the gas phase and in solution in which a large geometrical distortion from **FC** to $\mathbf{CI_F}$ can be accomplished. The other CI $\mathbf{CI_B}$ is energetically less favorable than $\mathbf{CI_F}$ and is not likely to compete against the quenching from $\mathbf{CI_F}$. However, this CI involves only CH out-

DOI: 10.1021/acs.jpca.5b07682
J. Phys. Chem. A 2015, 119, 11479−11487

of-plane motion that requires smaller geometry changes than the flat CI_F. Thus, CI_B can be reached even in solid and provides the quenching pathway in solid.

Molecule **2** with naphthaleneimide has only one conical intersection **CI** in the region that is lower in energy than the **FC** state. This **CI** shows a twisted structure with acene wings on the side of the tub-shaped cyclo-octatetraene ring and requires a large molecular motion. Thus, this **CI** is the quenching pathway in the gas phase and solution. However, in solid, this **CI** cannot be reached, and molecule **2** should be able to stay in the excited state and emit.

Different from the two molecules above, molecule **3** with anthraceneimide has no CI that is lower in energy than the FC state. Therefore, the quenching is not available in solution as well as in solid. Moreover, at the equilibrium structure in the S_1 state, transition from S_1 to S_0 is allowed by symmetry. Thus, this molecule is emissive even in solution.

We can conclude that the difference of emission behavior is determined by the difference of structures and energies of CIs. We succeeded in qualitatively explaining different emission behavior of three multiluminescent molecules. The present method of determining the structures and energies of low-energy CI using the GRRM strategy should be applicable to other photofunctional molecules, and such studies are in progress. Nonadiabatic molecular dynamics is required to quantitatively reproduce experimental results.

■ ASSOCIATED CONTENT

Supporting Information

The Supporting Information is available free of charge on the ACS Publications website at DOI: 10.1021/acs.jpca.5b07682.

Cartesian coordinates of all the optimized structures (PDF)

■ AUTHOR INFORMATION

Corresponding Author

*E-mail: morokuma@fukui.kyoto-u.ac.jp. Phone: +81-75-711-7843.

Notes

The authors declare no competing financial interest.

■ ACKNOWLEDGMENTS

The authors are grateful to Dr. Yu Harabuchi for his discussion on the SF-TDDFT method. This work was partly supported by Grants-in-Aid for Scientific Research (A) (No. 24245005 and 15H02158) to K.M. at Kyoto University. The Computer resources at the Academic Center for Computing and Media Studies (ACCMS) at Kyoto University and the Research Center of Computer Science (RCCS) at the Institute for Molecular Science are also acknowledged.

■ REFERENCES

(1) Yuan, C.; Saito, S.; Camacho, C.; Irle, S.; Hisaki, I.; Yamaguchi, S. A π-Conjugated System with Flexibility and Rigidity That Shows Environment-Dependent RGB Luminescence. *J. Am. Chem. Soc.* **2013**, *135*, 8842−8845.

(2) Yuan, C.; Saito, S.; Camacho, C.; Kowalczyk, T.; Irle, S.; Yamaguchi, S. Hybridization of a Flexible Cyclooctatetraene Core and Rigid Aceneimide Wings for Multiluminescent Flapping π Systems. *Chem.—Eur. J.* **2014**, *20*, 2193−2200.

(3) Yarkony, D. R. Diabolical Conical Intersections. *Rev. Mod. Phys.* **1996**, *68*, 985.

(4) Yarkony, D. R. Conical Intersections: Diabolical and Often Misunderstood. *Acc. Chem. Res.* **1998**, *31*, 511−518.

(5) Bernardi, F.; Olivucci, M.; Robb, M. A. Potential Energy Surface Crossings in Organic Photochemistry. *Chem. Soc. Rev.* **1996**, *25*, 321−328.

(6) Sobolewski, A. L.; Domcke, W.; Dedonder-Lardeux, C.; Jouvet, C. Excited-state Hydrogen Detachment and Hydrogen Transfer Driven by Repulsive 1πσ* States: A New Paradigm for Nonradiative Decay in Aromatic Biomolecules. *Phys. Chem. Chem. Phys.* **2002**, *4*, 1093−1100.

(7) Levine, B. G.; Martínez, T. J. Isomerization Through Conical Intersections. *Annu. Rev. Phys. Chem.* **2007**, *58*, 613−634.

(8) Nanbu, S.; Ishida, T.; Nakamura, H. Future Perspectives of Nonadiabatic Chemical Dynamics. *Chemical Science* **2010**, *1*, 663.

(9) Ohno, K.; Maeda, S. Global Reaction Route Mapping on Potential Energy Surfaces of Formaldehyde, Formic Acid, and Their Metal-Substituted Analogues. *J. Phys. Chem. A* **2006**, *110*, 8933.

(10) Maeda, S.; Morokuma, K. A Systematic Method for Locating Transition Structures of A+B→X Type Reactions. *J. Chem. Phys.* **2010**, *132*, 241102.

(11) Maeda, S.; Ohno, K.; Morokuma, K. Updated Branching Plane for Finding Conical Intersections without Coupling Derivative Vectors. *J. Chem. Theory Comput.* **2010**, *6*, 1538−1545.

(12) Maeda, S.; Ohno, K.; Morokuma, K. Systematic Exploration of the Mechanism of Chemical Reactions: the Global Reaction Route Mapping (GRRM) Strategy Using the ADDF and AFIR Methods. *Phys. Chem. Chem. Phys.* **2013**, *15*, 3683.

(13) Harabuchi, Y.; Maeda, S.; Taketsugu, T.; Minezawa, N.; Morokuma, K. Automated Search for Minimum Energy Conical Intersection Geometries between the Lowest Two Singlet States S_0/S_1-MECIs by the Spin-Flip TDDFT Method. *J. Chem. Theory Comput.* **2013**, *9*, 4116−4123.

(14) Maeda, S.; Harabuchi, Y.; Taketsugu, T.; Morokuma, K. Systematic Exploration of Minimum Energy Conical Intersection Structures near the Franck−Condon Region. *J. Phys. Chem. A* **2014**, *118*, 12050.

(15) Maeda, S.; Taketsugu, T.; Ohno, K.; Morokuma, K. From Roaming Atoms to Hopping Surfaces: Mapping Out Global Reaction Routes in Photochemistry. *J. Am. Chem. Soc.* **2015**, *137*, 3433.

(16) Andersson, K.; Malmqvist, P. Å.; Roos, B. O.; Sadlej, A. J.; Wolinski, K. Second-order Perturbation Theory with a CASSCF Reference Function. *J. Phys. Chem.* **1990**, *94* (14), 5483−5488. Finley, J.; Malmqvist, P.-Å.; Roos, B. O.; Serrano-Andrés, L. The Multi-state CASPT2Method. *Chem. Phys. Lett.* **1998**, *288*, 299−306.

(17) Nakano, H. Quasidegenerate Perturbation Theory with Multiconfigurational Self-consistent-field Reference Functions. *J. Chem. Phys.* **1993**, *99*, 7983.

(18) Shao, Y.; Head-Gordon, M.; Krylov, A. I. The Spin−flip Approach within Time-Dependent Density Functional Theory: Theory and applications to diradicals. *J. Chem. Phys.* **2003**, *118*, 4807.

(19) Minezawa, N.; Gordon, M. S. Optimizing Conical Intersections by Spin-Flip Density Functional Theory: Application to Ethylene. *J. Phys. Chem. A* **2009**, *113*, 12749.

(20) Minezawa, N.; Gordon, M. Photoisomerization of Stilbene: A Spin-Flip Density Functional Theory Approach. *J. Phys. Chem. A* **2011**, *115*, 7901−7911.

(21) Isegawa, M.; Truhlar, D. G. Valence Excitation Energies of Alkenes, Carbonyl Compounds, and Azabenzenes by Time-Dependent Density Functional theory: Linear response of the ground state compared to collinear and noncollinear spin-flip TDDFT with the Tamm-Dancoff approximation. *J. Chem. Phys.* **2013**, *138*, 134111.

(22) (a) Schmidt, M. W.; Baldridge, K. K.; Boatz, J. A.; Elbert, S. T.; Gordon, M. S.; Jensen, J. H.; Koseki, S.; Matsunaga, N.; Nguyen, K. A.; Su, S. J.; Windus, T. L.; Dupuis, M.; Montgomery, J. A. General Atomic and Molecular Electronic Structure System. *J. Comput. Chem.* **1993**, *14*, 1347. (b) Gordon, M. S.; Schmidt, M. W., Advances in electronic structure theory: GAMESS a decade later. In *Theory and Applications of Computational Chemistry: The First Forty Years*; Dykstra,

DOI: 10.1021/acs.jpca.5b07682
J. Phys. Chem. A 2015, 119, 11479−11487

C. E., Frenking, G., Kim, K. S., Scuseria, G. E., Eds.; Elsevier: Amsterdam, The Netherlands, 2005; p 1167.
(23) Maeda, S.; Osada, Y.; Morokuma, K.; Ohno, K. *GRRM version 1.30, a program for Global Reaction Route Mapping*; 2011.
(24) Tachibana, A.; Fukui, K. Differential Geometry of Chemically Reacting Systems. *Theoretica chimica acta* **1978**, *49*, 321.
(25) Garavelli, M.; Bernardi, F.; Cembran, A.; Castaño, O.; Frutos, L. M.; Merchán, M.; Olivucci, M. Cyclooctatetraene Computational Photo- and Thermal Chemistry: A Reactivity Model for Conjugated Hydrocarbons. *J. Am. Chem. Soc.* **2002**, *124*, 13770−13789.
(26) Bearpark, M. J.; Bernardi, F.; Clifford, S.; Olivucci, M.; Robb, M. A.; Vreven, T. Cooperating Rings in *cis*-Stilbene Lead to an S_0/S_1 Conical Intersection. *J. Phys. Chem. A* **1997**, *101*, 3841−3847.
(27) Jacquemin, D.; Wathelet, V.; Perpète, E. A.; Adamo, C. Extensive TD-DFT Benchmark: Singlet-Excited States of Organic Molecules. *J. Chem. Theory Comput.* **2009**, *5*, 2420−2435.

DOI: 10.1021/acs.jpca.5b07682
J. Phys. Chem. A 2015, 119, 11479−11487